A 1D Lagrangian scheme on NASG stiffened medium model with varying cross-section area

Wentian Wang
Ford Motor Company, Kanata, Ontario, Canada
Matei Radulescu
University of Ottawa, Ottawa, Ontario, Canada

1 Introduction

The computation of the hydrodynamics of compressible flows in dense media, such as solids, liquids and dense gases require an appropriate equation of state (EOS). For liquids and dense gases, a simple equation of state is the Noble-Abel Stiffened Gas (NASG) [1]. It offers the flexibility of treating flows with shock waves with accuracy while retaining the thermal behavior correctly [2] [3]. This is not the case for the simpler stiffened gas EOS commonly used in the literature, which do not permit thermodynamic ally correct formulations. The simplicity of the NASG EOS also permits to solve the Riemann problems in closed form, similar to the treatment of ideal gases [4]. The present study is the first implementation of such an exact Riemann solver for the NASG gas in a hydro-code and demonstration of the solution accuracy is two model problems: a multi-phase problem and in the geometrical implosion of shocks in liquids.

We are interested in solving problems that involve interfaces with multi-fluids for fusion research. We thus formulate our code in Lagrangian coordinates, such that interfaces can be modeled simply. Building on our recent work, such a Lagrangian approach [7] permits modeling piston-induced shock waves in 1D. In the present work, we extend the formalism to account for geometrical effects, such as flows with cylindrical or spherical symmetry or arbitrary quasi-1D flows, and extend the method to the NASG EOS.

Our preliminary demonstration of the computational methodology is for the problem of spherical shock implosion in liquids, for which an approximate model was recently proposed by us using Whithams approach of geometrical shock dynamics adapted to the NASG EOS. We further validate the code for the multi-fluid Riemann problem involving air and water.

2 Problems Addressing

This study investigates three cases of shock wave dynamics in NASG gases, described by the total energy equation:

$$e(p, v) = \frac{p + \gamma p_\infty}{\gamma - 1}(v - b) + q,$$

Correspondence to: wwang225@ford.com

while p_∞ and b are constants specific to the medium, and v, u and p represent specific volume, velocity and pressure, respectively. q is a constant to calibrate to unified the internal energy reference state. The first case involves a system with a constant cross-sectional area $\frac{\partial A}{\partial x} = 0$. The simulation begins with a Riemann problem initiated in air, modeled as a perfect gas, with the low-pressure side connected to water characterized by NASG parameters ($p_\infty = 7.02 \times 10^8 pa$, $b = 6.61 \times 10^{-4} m^3/kg$). This configuration ensures that a shock wave originating in the air ultimately propagates into the water medium.

At time zero, the initial conditions are divided into three regions by two contact surfaces. In the left region ($x \leq 19.5m$), the air is initialized with a high pressure $p_{left} = 2p_{atm} = 2.02 \times 10^5 pa$ and density $\rho_{left} = \rho_{air} = 1.29 kg/m^3$ driving a shock wave into the middle region. The middle region ($19.5m < x \leq 24.5m$) is filled with cool air at ambient pressure $p_{mid} = p_{atm}$, and density $\rho_{mid} = \rho_{air}$. The right region ($x > 24.5m$) contains water, initialized at equilibrium with the middle region at pressure $p_{right} = p_{atm}$, and density $\rho_{right} = \rho_{water} = 975 kg/m^3$.This problem was selected to evaluate the numerical scheme's performance and to examine wave and contact surface interactions between ideal gas and NASG mediums.

The second and third cases examine implosion dynamics in water under spherical symmetry, with weak shocks initialized at finite distances of $35m$ and $60m$, respectively. In these two problems, the center of the sphere is defined at $x = 0$, such that the radial coordinate $r = x$. For both cases, the initial state is set to ambient pressure $p = p_{atm}$ and the equilibrium density of water $\rho = \rho_{water}$. The second scenario involves a weak shock with an initial strength $z = 0.001$ while the third scenario features a strong shock with $z = 1$ where the shock strength z in the NASG gas is defined as

$$z = \frac{p_2 - p_1}{p_1 + p_\infty},$$

where p_1 and p_2 denote the ambient pressure and shocked pressure, respectively. These two cases were designed to assess the numerical scheme's capability to capture the dynamics of weak and strong imploding shocks. Furthermore, the shock strength evolution in these scenarios has been analyzed using several quasi-static analytical models. Comparisons between the simulation results and theoretical predictions [5] [8] highlight the reliability and accuracy of the proposed Lagrangian scheme in modeling implosion dynamics in NASG media.

3 Governing Equations and Numerical Setup

The quasi-one-dimensional governing equations for a NASG medium in a varying cross-sectional region, including spherical coordinates, are given as:

$$\frac{\partial v}{\partial t} + \frac{\partial}{\partial \phi}(-Au) = 0,$$

$$\frac{\partial u}{\partial t} + \frac{\partial p}{\partial \phi} = 0,$$

$$\frac{\partial e_{tot}}{\partial t} + \frac{\partial}{\partial \phi}(Apu) = 0,$$

Where A is the cross-section area which is a function of its position. ϕ is the Lagrangian space variable [7]. The numerical approach employs a second-order time-space reconstruction to compute the flux variables after applying a Godunov flux solver, which provides a first-order solution at the interfaces.The governing equations for the Godunov solver are detailed in Radulescu's work [4]. For all three problems,

the CourantFriedrichsLewy (CFL) number is set to 0.99. The left boundary condition is modeled as a reflective wall, while the right boundary condition allows free flow, implemented using a first-order polynomial interpolation to define the ghost cells. In two of the spherical coordinate simulations, the left boundary is positioned at a small finite distance from the sphere center ($x = 0.5m$). The left boundary cannot be placed directly at $x = r = 0$ due to the singularity at this point. Near the singular point, the shock strength theoretically approaches infinity and changes very rapidly. Therefore, the simulation does not fully resolve the shock convergence at the center but instead approximates this region by introducing a reflective inner wall (a small spherical surface) as the left boundary. The ability to accurately resolve the region near the singularity depends on the mesh grid size: finer grid resolution allows the left boundary to be positioned closer to the singular point.

4 Result and Discussion

Figure 1 illustrates the pressure evolution during the interaction of a shock wave with a stratified medium composed of high-pressure air, low-pressure air, and water described by the NASG model in Cartesian coordinates. At the interface between the high-pressure and low-pressure air, an initial shock wave propagates into the low-pressure air region, while an expansion wave travels back into the high-pressure air region. At $t \approx 0.013s$, as the shock wave enters the water region, significant refraction and reflection shock occur due to the stark differences in density and compressibility between the air and water. The reflected shock wave travels back toward the original air-air interface at $t \approx 0.020s$, triggering secondary interactions. Upon reaching this interface, the reflected wave induces a secondary expansion wave in the high-pressure air and a refracted shock wave propagating into the low-pressure air region. These successive interactions lead to the formation of complex wave structures, illustrating the intricate dynamics of shock wave behavior in stratified media. Notably, at $t = 0.028s$, the secondary expansion wave returns to the air-water interface, forming both a refracted expansion fan and a reflected expansion fan. From the slopes in the x-t diagram, it is evident that both the shock wave and the expansion wave exhibit strongly nonlinear wave speeds while propagating in the air. In contrast, the wave speeds for both the expansion wave and the shock wave remain nearly constant in the water. This behavior is attributed to the significantly large p_∞ in the NASG model for water, which causes shock waves with pressure variations on the order of atmospheric pressure to behave approximately as linear waves. When weak shock waves propagate through water, their lack of strong non-linearity leads to the formation of a shock layer with a fixed thickness in the numerical simulation. The thickness of this layer depends on the shock's non-linearity, numerical resolution, and factors such as the CFL number. Despite using a high CFL number of 0.99 in this simulation, significant numerical dissipation arises due to the noticeable pressure difference across the shock wave. However, the insufficient non-linearity of the weak shock fails to compress the dissipation effects into a thinner region.

Figure 2 shows the pressure evolution during the implosion process of shock waves in a spherical coordinate system. The left panel corresponds to a weak shock implosion, while the right panel shows a strong shock implosion. For the weak shock case (left), the wave front propagates inward with a nearly linear wave speed, as evidenced by the uniform slope in the x-t diagram. This linearity arises because the pressure gradient across the shock front remains small compared to $p_1 + p_\infty$, resulting in negligible non-linearity during propagation. Consequently, the weak shock can be approximated as a linear wave. During the implosion process, the intensity of the shock wave increases as it converges inward. Near r=0, the shock intensity grows sharply. This demonstrates the theoretical potential of a perfectly spherical imploding shock wave: even an initially weak shock can lead to nearly infinite temperature and pressure at the center of the sphere. Such amplification occurs due to the geometric focusing of the shock energy into an increasingly smaller volume as the wave approaches the center.

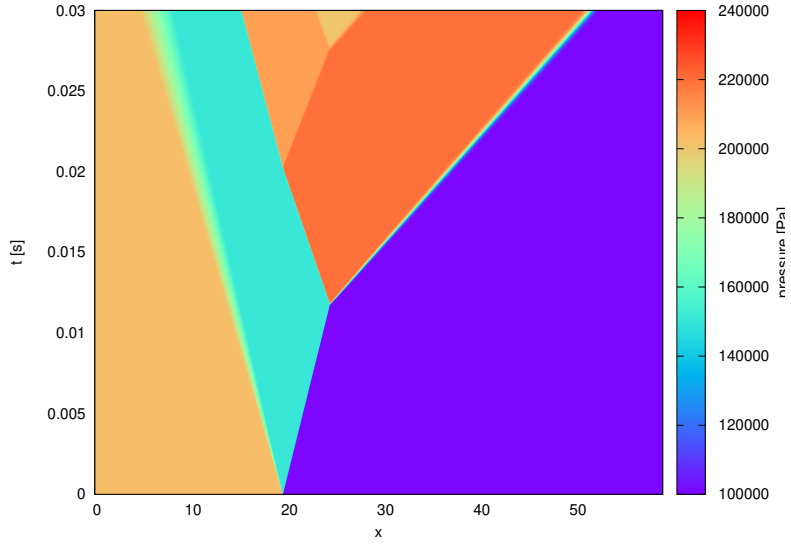

Figure 1: Reimann problem with a shock running from air to water

In contrast, the strong shock case (right) exhibits pronounced nonlinear behavior. The shock wave accelerates significantly as it converges toward the center, as reflected by the steepening of the slope in the x-t diagram. This non-linearity is driven by the high pressure gradients across the shock front, which amplify the compression and intensify the implosive dynamics. The result is a rapid increase in pressure near the center of the domain, with peak pressures several orders of magnitude higher than in the weak shock case. Upon reaching the center, the implosion generates a reflected shock wave that rapidly propagates outward at nearly infinite velocity. The pressure at the center decreases sharply after reflection but remains significantly higher than the pre-implosion pressure.

The reflected shock wave experiences a rapid decrease in intensity due to geometric expansion. Both the post-shock pressure and wave speed decline noticeably as the wavefront expands. Eventually, the shock wave speed stabilizes at the local speed of sound, marking the transition to a less nonlinear regime.

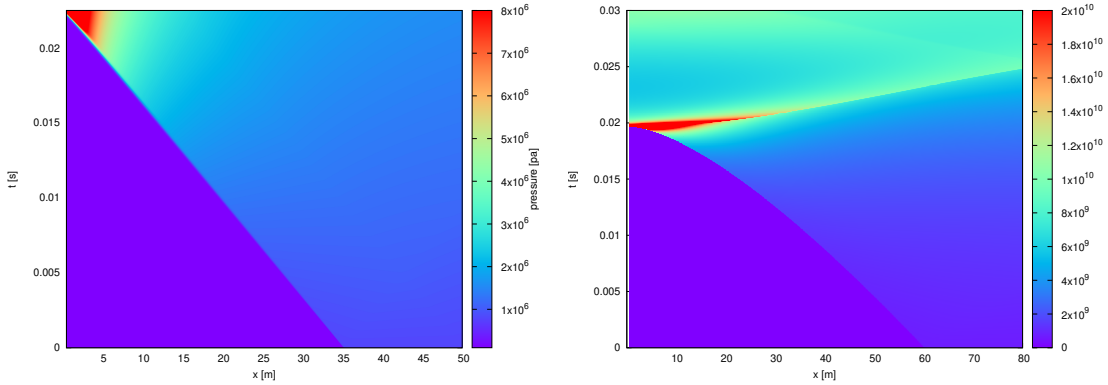

Figure 2: Pressure plot on spherical implosion problem with weak shock $z_0 = 0.001$(left) and strong shock $z_0 = 1$(right)

Figure 3 compares the relationship between the shock strength z and the ratio of the shock's cross-sectional area A to its initial cross-sectional area A_0 during the implosion process in a NASG medium. Since the simulation is spherical, the cross-sectional area is proportional to the square of the radius. The purple lines represent results obtained from numerical simulations, while the cyan and yellow lines correspond to two analytical models. The cyan line is based on the quasi-static approximation for

weak shock waves proposed by Radulescu (2020) [4], while the yellow line corresponds to the model developed by Whitham (1974) [8], which solves a complex ordinary differential equation (ODE) for z via numerical integration.

For the case with an initial shock strength of z=0.001 (left panel), the cyan and yellow lines almost perfectly overlap, indicating that the weak shock approximation aligns well with Whitham's model under low-strength conditions. However, the simulation results (purple line) show certain deviations from both analytical models, especially as the shock strength increases near the singular point. This discrepancy can be attributed to the numerical dissipation layer and limitations in capturing fine-scale effects in the simulation. Furthermore, as the shock approaches the singular point, the presence of the numerical dissipation layer makes it challenging to accurately determine the exact position of the shock. Even small positional deviations can lead to significant differences in the A/A_0 values on the logarithmic scale of the y-axis. This means that the right side of the curve heavily depends on the resolution of the simulation. Additionally, since the simulation represents a continuous process, while both theoretical models are based on the assumption of a quasi-static regime, the rapid increase in shock strength near the singular point deviates from the quasi-static assumption, further limiting the applicability of these models in this regime.

In contrast, for the case with an initial shock strength of z=1 (right panel), the weak shock approximation (cyan line) deviates significantly from the numerical results and Whithams model as the shock strength increases. This highlights the inherent limitations of the weak shock approximation when applied to high-strength shocks, where nonlinear effects dominate. Whithams model, although computationally intensive due to its reliance on ODE integration, better captures the behavior of high-strength shocks and aligns closely with the numerical results across the entire range of z.

In high-strength shock conditions, the thickness of the numerical dissipation layer decreases compared to the weak shock case. This reduction in dissipation thickness improves the accuracy of shock positioning under the same resolution, reducing the deviation between simulation results and theoretical predictions. However, the intensity of the shock changes much more rapidly in high-strength scenarios. At positions with similar area variation rates, the shock strength exhibits significantly larger changes, causing the actual behavior to deviate further from the quasi-static assumption. This more dynamic evolution of the shock strength is the primary reason for the observed differences between Whithams theoretical predictions and the numerical results.

These comparisons demonstrate that the weak shock approximation provides a simpler yet effective tool for analyzing low-strength shocks but fails to accurately describe scenarios involving high-strength shocks. Conversely, Whithams model remains robust across a broader range of shock intensities but requires more sophisticated numerical treatment.

5 Conclusion

The present study extends the original 1-dimensional Lagrangian scheme by incorporating the NASG gas model and a variable cross-sectional area framework to numerically investigate implosion problems in water. This approach provides a simple and effective numerical method for studies involving NASG fluids and varying cross-sectional geometries. For low-intensity shocks, where non-linearity is less pronounced, higher resolution is required to accurately capture the detailed shock position. In contrast, for high-intensity shocks, this method proves to be a reliable tool for theoretical investigations even under lower resolution conditions, owing to the reduced sensitivity to numerical dissipation.

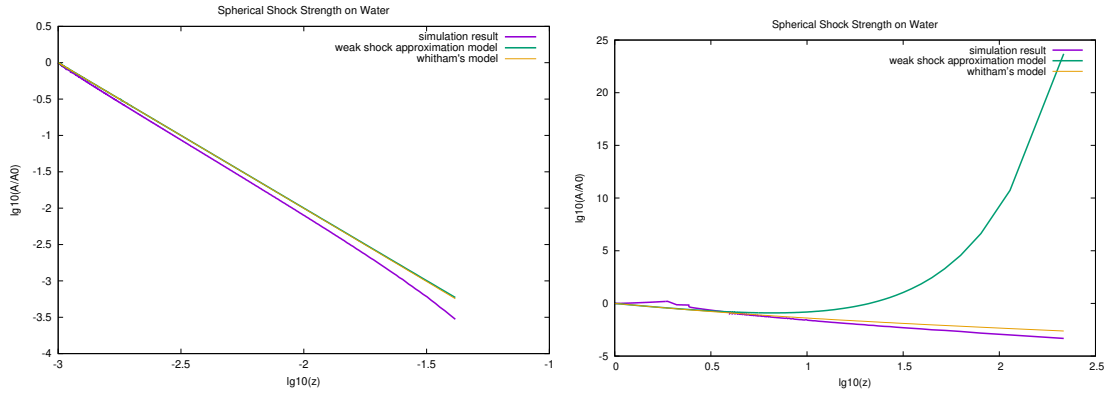

Figure 3: Comparison of shock strength plot in NASG medium with the varying cross-section area in quasi-1D problem

References

[1] Le Mtayer, Olivier, and Richard Saurel. "The Noble-Abel stiffened-gas equation of state." Physics of Fluids 28.4 (2016).

[2] Furfaro, Damien, et al. "Towards sodium combustion modeling with liquid water." Journal of Computational Physics 403 (2020): 109060.

[3] P. Boivin, M. A. Cannac, and O. Le Mtayer, A thermodynamic closure for the simulation of multiphase reactive flows, Int. J. Therm. Sci. 137, 640649 (2019).

[4] M. I. Radulescu. Compressible flow in a Noble-Abel stiffened gas fluid. Physics of Fluids, 32(5):056101, 2020.

[5] Ioan Rdulescu, Matei. "Geometrical Shock Dynamics in a Noble-Abel stiffened gas medium." arXiv e-prints (2023): arXiv-2311.

[6] W. Wang, J. G. McDonald, and M. I. Radulescu, "Role of gasdynamic wave fluctuations in shock induced ignition and transition to detonation: the hotspot cascade mechanism," *Proceedings of the 27th International Colloquium on the Dynamics of Explosions and Reactive Systems*, Paper 322, 2019.

[7] Wang, Wentian, James McDonald, and Matei Ioan Radulescu. "Shock induced ignition and transition to detonation in the presence of mechanically induced non-linear acoustic forcing." arXiv preprint arXiv:2312.05443 (2023).

[8] G. B. Whitham, *Linear and Nonlinear Waves*. Wiley, 1974.